Fluctuation-driven topological transition of binary condensates in optical lattices

K. Suthar,[1,2] Arko Roy,[1,2] and D. Angom[1]
[1]*Physical Research Laboratory, Navrangpura, Ahmedabad-380009, Gujarat, India*
[2]*Indian Institute of Technology, Gandhinagar, Ahmedabad-382424, Gujarat, India*
(Received 29 December 2014; published 13 April 2015)

We show the emergence of a third Goldstone mode in binary condensates at phase separation in quasi-one-dimensional (quasi-1D) optical lattices. We develop the coupled discrete nonlinear Schrödinger equations using Hartree-Fock-Bogoliubov theory with the Popov approximation in the Bose-Hubbard model to investigate the mode evolution at zero temperature, in particular, as the system is driven from the miscible to the immiscible phase. We demonstrate that the position exchange of the species in the ^{87}Rb-^{85}Rb system is accompanied by a discontinuity in the excitation spectrum. Our results show that, in quasi-1D optical lattices, the presence of the fluctuations dramatically changes the geometry of the ground-state density profile of two-component Bose-Einstein condensates.

DOI: 10.1103/PhysRevA.91.043615 PACS number(s): 67.85.Bc, 42.50.Lc, 67.85.Fg, 67.85.Hj

I. INTRODUCTION

Ultracold dilute atomic Bose gases in low dimensions have been the subject of growing interest over the last few decades. These are an ideal platform to probe many-body phenomena where quantum fluctuations play a crucial role [1,2]. In particular, optical lattices serve as an excellent and versatile tool for studying the physics of strongly correlated systems and other phenomena in condensed matter physics [3,4]. A variety of experimental techniques have been used to load and manipulate Bose-Einstein condensates (BECs) in optical lattices [5–8]. These have helped to explore quantum phase transitions [9], in particular the superfluid (SF)–Mott insulator (MI) transition [10–13]. The characteristics of the SF phase, such as coherence [14,15], collective modes [16], and transport [17,18] have also been studied. The center-of-mass dipole oscillation of a BEC in a cigar-shaped lattice potential has been experimentally studied in detail [19]. In such systems, a decrease in the Kohn mode frequency has been reported in Ref. [20] which has been justified in Ref. [21] as an increase of the effective mass due to the lattice potential. On the theoretical front, the low-lying collective excitations of a trapped Bose gas in a periodic lattice potential have been studied in Refs. [22–25] using the Bose-Hubbard (BH) model [26].

The two-component BECs (TBECs), on the other hand, exhibit a unique property that they can be phase separated [27]. There have been numerous experimental and theoretical investigations of binary mixtures of BECs over the last few years. Experimentally, it is possible to vary the interactions through the Feshbach resonance [28,29], and drive the binary mixture from the miscible to the immiscible phase or vice versa. Among the various lines of investigation, the theoretical studies of the stationary states [30], dynamical instabilities [31,32], and the collective excitations [33,34] of TBECs are noteworthy. Furthermore, in optical lattices TBECs have also been observed in recent experiments [35,36]. Theoretical studies of TBECs in optical lattices [37–40] and, in particular, phase separation [41–43] and dynamical instabilities [44] have also been carried out. Despite all these theoretical and experimental advances, the study of collective excitations of TBECs in optical lattices is yet to be explored. This is the research gap addressed in the present work.

In this paper, we report the development of coupled discrete nonlinear Schrödinger equations (DNLSEs) of TBECs in optical lattices under the Hartree-Fock-Bogoliubov (HFB)–Popov approximation [45]. We use this theory to study the ground-state density profiles and the quasiparticle spectrum of ^{87}Rb-^{85}Rb and ^{133}Cs-^{87}Rb TBECs at zero temperature. We focus, in particular, on the evolution of the quasiparticle as the TBEC is driven from the miscible to the immiscible phase. This is possible by tuning either the intra- or interspecies interaction strengths. The two systems considered correspond to these possibilities. The fluctuation- and interaction-induced effects on the collective excitation spectra and topological change in the density profiles are the major findings of our present study. It deserves to be mentioned here that for systems without a lattice potential, at equilibrium, recent works have shown the existence of additional Goldstone modes in TBECs at phase separation [46] and complex eigenenergies due to quantum fluctuations [47].

The paper is organized as follows. Section II describes the tight-binding approximation for a trapped BEC in a one-dimensional (1D) lattice potential. In Sec. III we present the HFB-Popov theory to determine the quasiparticle energies and mode functions of single-component BECs and TBECs at finite temperature. The results of our studies are presented in Sec. IV. Finally, we highlight the key results of our work in Sec. V.

II. QUASI-1D OPTICAL LATTICE

We consider a Bose-Einstein condensate, held within a highly anisotropic cigar-shaped harmonic potential with trapping frequencies $\omega_x = \omega_y = \omega_\perp \gg \omega_z$. In this case we can integrate out the condensate wave function along the x and y directions and reduce it to a quasi-1D condensate. In the mean-field approximation, the grand-canonical Hamiltonian, in the second-quantized form, of the bosonic atoms in an external potential plus lattice is

given by

$$\hat{H} = \int dz\hat{\Psi}^{\dagger}(z)\Big(-\frac{\hbar^2}{2m}\frac{\partial^2}{\partial z^2} + V_{\text{latt}}(z)\Big)\hat{\Psi}(z) + \int dz(V_{\text{ext}} - \mu)\hat{\Psi}^{\dagger}(z)\hat{\Psi}(z) + \frac{1}{2}\int dzdz'\hat{\Psi}^{\dagger}(z)\hat{\Psi}^{\dagger}(z')U(z-z')\hat{\Psi}(z)\hat{\Psi}(z'), \quad (1)$$

where $\hat{\Psi}(z)$ and $\hat{\Psi}^{\dagger}(z)$ are the bosonic field operators which obey the Bose commutation relations, m is the atomic mass of the species, V_{latt} is the periodic lattice potential, V_{ext} is the external trapping potential, and μ is the chemical potential. Here, the interaction potential is given by $U(z-z') = U\delta(z-z')$, where $U = 2\sqrt{\lambda\kappa}\hbar^2 N a_s/m$, with N as the total number of atoms, and $\lambda = \omega_x/\omega_z$ and $\kappa = \omega_y/\omega_z$ are the anisotropy parameters along the x and y directions, respectively. Here a_s is the s-wave scattering length, which is repulsive ($a_s > 0$) in the present work. The net external potential is

$$V = V_{\text{ext}} + V_{\text{latt}} = \tfrac{1}{2}m\omega_z^2 z^2 + V_0\sin^2(kz), \quad (2)$$

where $V_0 = sE_R$ is the optical lattice depth with s and E_R as the lattice depth scaling parameter and the recoil energy of the laser light photon, respectively. The wave number of the counterpropagating laser beams, which are used to create a periodic lattice potential, is $k = \pi/a$ with $a = \lambda_L/2$ the lattice spacing and λ_L the wavelength of the laser light. The energy barrier between adjacent lattice sites is expressed in units of the recoil energy $E_R = \hbar^2k^2/2m$. In the tight-binding approximation, valid when $\mu \ll V_0$, the 1D field operator can be written as [48]

$$\hat{\Psi}(z) = \sum_j \hat{a}_j\phi_j(z), \quad (3)$$

where $\hat{a}_j$ is the annihilation operator corresponding to the jth site, and the spatial part $\phi_j(z) = \phi(z - ja)$ is the orthonormal Gaussian orbital of the lowest vibrational band centered at the jth lattice site, with $\int dz\phi^*_{j\pm1}(z)\phi_j(z) = 0$ and $\int dz|\phi_j(z)|^2 = 1$. By using the above ansatz in $\hat{H}$ and considering only the nearest-neighbor tunneling we obtain the Bose-Hubbard Hamiltonian.

III. HFB-POPOV APPROXIMATION

A. Single-component BEC in optical lattices

The BH Hamiltonian describes the dynamics of 1D optical lattices when only the lowest band or the lowest vibrational level of the site is occupied. In this case the tight-binding approximation [49] is valid, and the BH Hamiltonian of the system is

$$\hat{H} = -J\sum_{\langle jj'\rangle}\hat{a}_j^{\dagger}\hat{a}_{j'} + \sum_j\Big[(\epsilon_j - \mu)\hat{a}_j^{\dagger}\hat{a}_j + \frac{1}{2}U\hat{a}_j^{\dagger}\hat{a}_j^{\dagger}\hat{a}_j\hat{a}_j\Big], \quad (4)$$

where the index j runs over the lattice sites, $\langle jj'\rangle$ represents the nearest-neighbor sum, and $\hat{a}_j$ ($\hat{a}_j^{\dagger}$) is the bosonic annihilation (creation) operator of a bosonic atom at the jth lattice site. Here $J = -\int dz\phi^*_{j+1}(z)[-(\hbar^2/2m)(\partial^2/\partial z^2) + V_0\sin^2(2\pi z/\lambda_L)]\phi_j(z)$ is the tunneling matrix element between adjacent sites, $\epsilon_j = \int dzV_{\text{ext}}(z)|\phi_j(z)|^2$ is the energy offset of the jth lattice site, and $U = (2\sqrt{\lambda\kappa}\hbar^2 N a_s/m)\int dz|\phi_j(z)|^4$ is the on-site interaction strength of atoms occupying the jth lattice site. The offset energy can also be expressed as $\epsilon_j = j^2\Omega$; here, $\Omega = m\omega_z^2a^2/2$ is the energy cost of moving a boson from the central site to its nearest-neighbor site. To take into account the quantum fluctuations and thermal effects in the description of the system, we decompose the Bose field operator of each lattice site j in terms of a complex mean-field part c_j and a fluctuation operator $\hat{\varphi}_j$, as $\hat{a}_j = (c_j + \hat{\varphi}_j)e^{-i\mu t/\hbar}$. Using this field operator in the BH Hamiltonian, we get

$$\hat{H} = H_0 + \hat{H}_1 + \hat{H}_2 + \hat{H}_3 + \hat{H}_4, \quad (5)$$

with

$$H_0 = -J\sum_{\langle jj'\rangle}c_j^*c_{j'} + \sum_j\Big[(\epsilon_j - \mu)|c_j|^2 + \frac{1}{2}U|c_j|^4\Big], \quad (6a)$$

$$\hat{H}_1 = -J\sum_{\langle jj'\rangle}\hat{\varphi}_jc_{j'}^* + \sum_j(\epsilon_j - \mu + U|c_j|^2)c_j^*\hat{\varphi}_j + \text{H.c.}, \quad (6b)$$

$$\hat{H}_2 = -J\sum_{\langle jj'\rangle}\hat{\varphi}_j^{\dagger}\hat{\varphi}_{j'} + \sum_j(\epsilon_j - \mu)\hat{\varphi}_j^{\dagger}\hat{\varphi}_j + \frac{U}{2}\sum_j\big(\hat{\varphi}_j^{\dagger 2}c_j^2 + \hat{\varphi}_j^2c_j^{*2} + 4|c_j|^2\hat{\varphi}_j^{\dagger}\hat{\varphi}_j\big), \quad (6c)$$

$$\hat{H}_3 = U\sum_j\hat{\varphi}_j^{\dagger}\hat{\varphi}_j^{\dagger}\hat{\varphi}_jc_j + \text{H.c.}, \quad (6d)$$

$$\hat{H}_4 = \frac{U}{2}\sum_j\hat{\varphi}_j^{\dagger}\hat{\varphi}_j^{\dagger}\hat{\varphi}_j\hat{\varphi}_j, \quad (6e)$$

where the subscript of the various terms indicates the order of fluctuation operators and H.c. stands for the Hermitian conjugate. To study the system without quantum fluctuation at $T = 0$ K, we consider terms up to second order in $\hat{\varphi}_j$ and neglect the higher-order terms (third and fourth order). The lowest-order term of the Hamiltonian describes the condensate part of the system. The minimization of H_0 with respect to the variation in the complex amplitude c_j^* gives the time-independent DNLSE, which can be written as

$$\mu c_j = -J(c_{j-1} + c_{j+1}) + \big(\epsilon_j + Un_j^c\big)c_j, \quad (7)$$

with the condensate density $n_j^c = |c_j|^2$. The quadratic Hamiltonian $\hat{H}_2$ is the leading-order term which describes the noncondensate part, since the variation in $\hat{H}_1$ vanishes because c_j is a stationary solution of the DNLSE. The minimization of $\hat{H}_2$ yields the governing equation for the noncondensate given by

$$\mu\hat{\varphi}_j = -J(\hat{\varphi}_{j-1} + \hat{\varphi}_{j+1}) + \big(\epsilon_j + 2Un_j^c\big)\hat{\varphi}_j + Uc_j^2\hat{\varphi}_j^{\dagger}. \quad (8)$$

The quadratic Hamiltonian can be diagonalized using the Bogoliubov transformation

$$\hat{\varphi}_j = \sum_l\big[u_j^l\hat{\alpha}_le^{-i\omega_lt} - v_j^{*l}\hat{\alpha}_l^{\dagger}e^{i\omega_lt}\big], \quad (9a)$$

$$\hat{\varphi}_j^\dagger = \sum_l \left[u_j^{*l}\hat{\alpha}_l^\dagger e^{i\omega_l t} - v_j^l \hat{\alpha}_l e^{-i\omega_l t}\right], \tag{9b}$$

where u_j^l and v_j^l are the quasiparticle amplitudes, $\omega_l = E_l/\hbar$ is the lth quasiparticle mode frequency with E_l as the mode energy, and $\hat{\alpha}_l$ ($\hat{\alpha}_l^\dagger$) are the quasiparticle annihilation (creation) operators, which satisfy the Bose commutation relations. The quasiparticle amplitudes satisfy the following normalization conditions:

$$\sum_j \left(u_j^{*l}u_j^{l'} - v_j^{*l}v_j^{l'}\right) = \delta_{ll'}, \tag{10a}$$

$$\sum_j \left(u_j^l v_j^{l'} - v_j^{*l}u_j^{*l'}\right) = 0. \tag{10b}$$

By using the definition of $\hat{\varphi}_j$ from Eq. (9) in $\hat{H}_2$ [Eq. 6(c)] and the above conditions, we get the following Bogoliubov–de Gennes (BdG) equations

$$E_l u_j^l = -J\left(u_{j-1}^l + u_{j+1}^l\right) + \left[2Un_j^c + (\epsilon_j - \mu)\right]u_j^l - Uc_j^2 v_j^l, \tag{11a}$$

$$E_l v_j^l = J\left(v_{j-1}^l + v_{j+1}^l\right) - \left[2Un_j^c + (\epsilon_j - \mu)\right]v_j^l + Uc_j^{*2}u_j^l. \tag{11b}$$

This set of coupled equations describes the quasiparticles of the condensate in the optical lattice without considering the quantum fluctuations.

To investigate the effect of fluctuation and finite temperature we include the higher-order terms ($\hat{H}_3$ and $\hat{H}_4$) of the fluctuation operator in the Hamiltonian. We treat these terms in the self-consistent mean-field approximation [45] such that $\hat{\varphi}_j^\dagger\hat{\varphi}_j\hat{\varphi}_j \approx 2\tilde{n}_j\hat{\varphi}_j + \tilde{m}_j\hat{\varphi}_j^\dagger$ and $\hat{\varphi}_j^\dagger\hat{\varphi}_j^\dagger\hat{\varphi}_j\hat{\varphi}_j \approx 4\tilde{n}_j\hat{\varphi}_j^\dagger\hat{\varphi}_j + \tilde{m}_j\hat{\varphi}_j^\dagger\hat{\varphi}_j^\dagger + \tilde{m}_j^*\hat{\varphi}_j\hat{\varphi}_j - (2\tilde{n}_j^2 + |\tilde{m}_j|^2)$, where $\tilde{n}_j = \langle\hat{\varphi}_j^\dagger\hat{\varphi}_j\rangle$ and $\tilde{m}_j = \langle\hat{\varphi}_j\hat{\varphi}_j\rangle$ are the excited population (noncondensate) density and anomalous density at the jth site, respectively. In the HFB-Popov approximation, where the anomalous density is neglected, the corrections from higher-order terms yield the modified DNLSE

$$\mu' c_j = -J(c_{j-1} + c_{j+1}) + \left[\epsilon_j + U\left(n_j^c + 2\tilde{n}_j\right)\right]c_j, \tag{12}$$

where μ' is the modified chemical potential. The total density is $n = \sum_j(n_j^c + \tilde{n}_j)$. The diagonalization of the modified Hamiltonian leads to the following HFB-Popov equations:

$$E_l u_j^l = -J\left(u_{j-1}^l + u_{j+1}^l\right) + \left[2U\left(n_j^c + \tilde{n}_j\right) + (\epsilon_j - \mu')\right]u_j^l - Uc_j^2 v_j^l, \tag{13a}$$

$$E_l v_j^l = J\left(v_{j-1}^l + v_{j+1}^l\right) - \left[2U\left(n_j^c + \tilde{n}_j\right) + (\epsilon_j - \mu')\right]v_j^l + Uc_j^{*2}u_j^l, \tag{13b}$$

with the noncondensate density at the jth lattice site given by

$$\tilde{n}_j = \sum_l \left[\left(|u_j^l|^2 + |v_j^l|^2\right)N_0(E_l) + |v_j^l|^2\right], \tag{14}$$

where $N_0(E_l) = \langle\hat{\alpha}_l^\dagger\hat{\alpha}_l\rangle = (e^{\beta E_l} - 1)^{-1}$ is the Bose-Einstein distribution function of the quasiparticle state with real and positive mode energy E_l. The coupled equations (12) and (13) are solved iteratively until the solutions converge to the desired accuracy. It is important to note that, at $T = 0$ K, $N_0(E_l)$ in the above equation vanishes. The noncondensate density, then, has a contribution from only the quantum fluctuations, which is given by

$$\tilde{n}_j = \sum_l |v_j^l|^2. \tag{15}$$

Therefore, we solve the equations self-consistently in the presence of the quantum fluctuations.

B. Two-component BEC in optical lattices

For a two-species condensate, the 1D second-quantized grand-canonical Hamiltonian is given by

$$\hat{H} = \sum_{i=1}^{2}\int dz\hat{\Psi}_i^\dagger(z)\Big[-\frac{\hbar^2}{2m_i}\frac{\partial^2}{\partial z^2} + V^i(z) - \mu_i + \frac{U_{ii}}{2}\hat{\Psi}_i^\dagger(z) \times \hat{\Psi}_i(z)\Big]\hat{\Psi}_i(z) + U_{12}\int dz\hat{\Psi}_1^\dagger(z)\hat{\Psi}_2^\dagger(z)\hat{\Psi}_1(z)\hat{\Psi}_2(z), \tag{16}$$

where $i = 1,2$ denotes the species index, the $\hat{\Psi}_i$'s are the annihilation field operators for the two different species, μ_i is the chemical potential of the ith species, U_{ii} are the intraspecies interaction parameters, and U_{12} is the interspecies interaction parameter with the m_i's as the atomic masses of the species. Here, we consider repulsive interactions $U_{ii}, U_{12} > 0$. The external potential V^i is the sum of the harmonic and periodic optical lattice potentials. It is given by

$$V^i = V_{\text{ext}}^i + V_{\text{latt}}^i = \frac{1}{2}m_i\omega_{z_i}^2 z_i^2 + V_0\sin^2(2\pi z_i/\lambda_L). \tag{17}$$

In the present work, we consider the same external potential for both the species. The depth of the lattice potential is also the same for both species and is $V_0 = sE_R$ with $E_R = \hbar^2k^2/2m_1$. If the lattice is deep enough, the tight-binding approximation is valid, and the bosons can be assumed to occupy the lowest vibrational band only. Under this approximation, the Bose field operator for the two species can be expanded as

$$\hat{\Psi}_i(z) = \sum_j \hat{a}_{ij}\phi_{ij}(z), \tag{18}$$

where the $\hat{a}_{ij}$'s are the annihilation operators and the $\phi_{ij}(z)$'s are the orthonormal Gaussian bases of the two species. It is worth mentioning here that the width of the basis function depends on the mass of the species and the natural frequency of the lattice potential. In the present case, the frequency plays a dominant role over the mass of the constituent species. Hence the widths of the Gaussian basis functions are taken to be identical for both species, even when m_1 and m_2 are widely different. The BH Hamiltonian for two species can be obtained by using the above ansatz in the Hamiltonian Eq. (16). We then obtain the many-body Hamiltonian governing the system of a

binary BEC in a quasi-1D optical lattice as

$$\hat{H} = \sum_{i=1}^{2}\left[-\sum_{\langle jj'\rangle} J_i \hat{a}_{ij}^{\dagger}\hat{a}_{ij'} + \sum_j \left(\epsilon_j^{(i)} - \mu_i\right)\hat{a}_{ij}^{\dagger}\hat{a}_{ij}\right] + \frac{1}{2}\sum_{i=1}^{2} U_{ii}\sum_j \hat{a}_{ij}^{\dagger}\hat{a}_{ij}^{\dagger}\hat{a}_{ij}\hat{a}_{ij} + U_{12}\sum_j \hat{a}_{1j}^{\dagger}\hat{a}_{1j}\hat{a}_{2j}^{\dagger}\hat{a}_{2j}. \tag{19}$$

Here J_i are the tunneling matrix elements, and $\epsilon_j^{(i)}$ is the offset energy of species i at the jth lattice site. In the mean-field approximation, using the Bogoliubov approximation as in a single-species condensate, we decompose the operators of both species as $\hat{a}_{1j} = (c_j + \hat{\varphi}_{1j})e^{-i\mu_1 t/\hbar}$ and $\hat{a}_{2j} = (d_j + \hat{\varphi}_{2j})e^{-i\mu_2 t/\hbar}$. We use these definitions in the BH Hamiltonian [Eq. (19)] and then decompose the Hamiltonian into different terms according to the order of the noncondensate operator they contain. The minimization of the lowest-order term gives the stationary-state equations or time-independent coupled DNLSEs, and these are given by

$$\mu_1 c_j = -J_1(c_{j-1} + c_{j+1}) + \left[\epsilon_j^{(1)} + U_{11}n_{1j}^c + U_{12}n_{2j}^c\right]c_j, \tag{20a}$$

$$\mu_2 d_j = -J_2(d_{j-1} + d_{j+1}) + \left[\epsilon_j^{(2)} + U_{22}n_{2j}^c + U_{12}n_{1j}^c\right]d_j, \tag{20b}$$

where $n_{1j}^c = |c_j|^2$ and $n_{2j}^c = |d_j|^2$ are the condensate densities of the first and second species, respectively. The noncondensate part of the TBEC is obtained by the minimization of the quadratic Hamiltonian

$$\mu_1\hat{\varphi}_{1j} = -J_1(\hat{\varphi}_{1,j-1} + \hat{\varphi}_{1,j+1}) + \left[\epsilon_j^{(1)} + 2U_{11}n_{1j}^c\right]\hat{\varphi}_{1j} + U_{11}c_j^2\hat{\varphi}_{1j}^{\dagger} + U_{12}\left(n_{2j}^c\hat{\varphi}_{1j} + d_j^* c_j\hat{\varphi}_{2j} + d_j c_j\hat{\varphi}_{2j}^{\dagger}\right), \tag{21a}$$

$$\mu_2\hat{\varphi}_{2j} = -J_2(\hat{\varphi}_{2,j-1} + \hat{\varphi}_{2,j+1}) + \left[\epsilon_j^{(2)} + 2U_{22}n_{2j}^c\right]\hat{\varphi}_{2j} + U_{22}d_j^2\hat{\varphi}_{2j}^{\dagger} + U_{12}\left(n_{1j}^c\hat{\varphi}_{2j} + c_j^* d_j\hat{\varphi}_{1j} + c_j d_j\hat{\varphi}_{1j}^{\dagger}\right). \tag{21b}$$

The Bogoliubov transformation equations of the TBEC, which couple the positive- and negative-energy mode excitations, are

$$\hat{\varphi}_{ij} = \sum_l \left[u_{ij}^l\hat{\alpha}_l e^{-i\omega_l t} - v_{ij}^{*l}\hat{\alpha}_l^{\dagger}e^{i\omega_l t}\right], \tag{22a}$$

$$\hat{\varphi}_{ij}^{\dagger} = \sum_l \left[u_{ij}^{*l}\hat{\alpha}_l^{\dagger}e^{i\omega_l t} - v_{ij}^l\hat{\alpha}_l e^{-i\omega_l t}\right], \tag{22b}$$

where u_{ij}^l and v_{ij}^l are the quasiparticle amplitudes for the first ($i = 1$) and second ($i = 2$) species. The above transformation diagonalizes the quadratic Hamiltonian and gives the Bogoliubov–de Gennes equations at $T = 0$ K for the two-component system. The inclusion of the higher-order terms of the perturbation or fluctuation in the quadratic Hamiltonian gives the HFB-Popov equations for the two-component BEC,

$$E_l u_{1,j}^l = -J_1\left(u_{1,j-1}^l + u_{1,j+1}^l\right) + \mathcal{U}_1 u_{1,j}^l - U_{11}c_j^2 v_{1,j}^l + U_{12}c_j\left(d_j^* u_{2,j}^l - d_j v_{2,j}^l\right), \tag{23a}$$

$$E_l v_{1,j}^l = J_1\left(v_{1,j-1}^l + v_{1,j+1}^l\right) + \underline{\mathcal{U}}_1 v_{1,j}^l + U_{11}c_j^{*2}u_{1,j}^l - U_{12}c_j^*\left(d_j v_{2,j}^l - d_j^* u_{2,j}^l\right), \tag{23b}$$

$$E_l u_{2,j}^l = -J_2\left(u_{2,j-1}^l + u_{2,j+1}^l\right) + \mathcal{U}_2 u_{2,j}^l - U_{22}d_j^2 v_{2,j}^l + U_{12}d_j\left(c_j^* u_{1,j}^l - c_j v_{1,j}^l\right), \tag{23c}$$

$$E_l v_{2,j}^l = J_2\left(v_{2,j-1}^l + v_{2,j+1}^l\right) + \underline{\mathcal{U}}_2 v_{2,j}^l + U_{22}d_j^{*2}u_{2,j}^l - U_{12}d_j^*\left(c_j v_{1,j}^l - c_j^* u_{1,j}^l\right), \tag{23d}$$

where $\mathcal{U}_1 = 2U_{11}(n_{1j}^c + \tilde{n}_{1j}) + U_{12}(n_{2j}^c + \tilde{n}_{2j}) + (\epsilon_j^{(1)} - \mu_1)$ and $\mathcal{U}_2 = 2U_{22}(n_{2j}^c + \tilde{n}_{2j}) + U_{12}(n_{1j}^c + \tilde{n}_{1j}) + (\epsilon_j^{(2)} - \mu_2)$ with $\underline{\mathcal{U}}_i = -\mathcal{U}_i$. The density of the noncondensate atoms at the jth lattice site is

$$\tilde{n}_{ij} = \sum_l \left[\left(|u_{ij}^l|^2 + |v_{ij}^l|^2\right)N_0(E_l) + |v_{ij}^l|^2\right], \tag{24}$$

with $N_0(E_l)$ as the Bose factor of the system with energy E_l at temperature T. At $T = 0$ K the noncondensate part reduces to the quantum fluctuations

$$\tilde{n}_{ij} = \sum_l |v_{ij}^l|^2. \tag{25}$$

If we neglect quantum fluctuations (the noncondensate part), the HFB-Popov equations (23) are the BdG equations for a binary BEC.

IV. RESULTS AND DISCUSSION

A. Numerical details

We solve the scaled coupled DNLSEs using the fourth-order Runge-Kutta method to find the equilibrium state of harmonically trapped binary condensates in optical lattices. We start the calculations for $T = 0$ K by ignoring the quantum fluctuations at each lattice site. The initial complex amplitudes of both species c_j and d_j are chosen as $1/\sqrt{N_{\text{latt}}}$, with N_{latt} as the total number of lattice sites. The advantage of this choice is that the amplitudes are normalized. We then use imaginary-time propagation of the DNLSEs (20) to find the stationary ground-state wave function of the TBEC. In the tight-binding limit, the condensate wave function can be defined as the superposition of the basis functions as shown in Eq. (18). The basis function is chosen as the ground state, which is a Gaussian function, of the lowest-energy band [48]. The width of the function is a crucial parameter as it affects the overlap of the Gaussian orbitals at each lattice site. The correct estimation of the width is required in order to obtain orthonormal basis functions [50]. Furthermore, to study the excitation spectrum, we cast Eqs. (23) as a matrix eigenvalue equation. The matrix is $4N_{\text{latt}} \times 4N_{\text{latt}}$, non-Hermitian, nonsymmetric, and may have complex eigenvalues. To diagonalize the matrix and to find the quasiparticle energies E_l and amplitudes u_{ij}^l and v_{ij}^l, we use the routine ZGEEV from the LAPACK library [51]. In the later part of the work, when we include the effect of the

quantum fluctuations, we need to solve Eqs. (20) and (23) self-consistently. For this we iterate the solution until we reach the desired convergence in the number of condensate and noncondensate atoms. In this process, sometimes we encounter severe oscillations in the number of atoms. To damp these oscillations and accelerate convergence we employ a successive over- (under-) relaxation technique for updating the condensate (noncondensate) atom densities [52]. The new solutions after the iteration cycle (IC) are given by

$$c^{\rm new}_{j,{\rm IC}} = r^{\rm ov} c_{j,{\rm IC}} + (1 - r^{\rm ov}) c_{j,{\rm IC}-1}, \tag{26a}$$

$$\tilde{n}^{\rm new}_{j,{\rm IC}} = r^{\rm un} \tilde{n}_{j,{\rm IC}} + (1 - r^{\rm un}) \tilde{n}_{j,{\rm IC}-1}, \tag{26b}$$

where $r^{\rm ov} > 1$ ($r^{\rm un} < 1$) is the over- (under-) relaxation parameter. After the condensate and noncondensate densities converge, we compute low-lying mode energies and amplitudes u^l_{ij} and v^l_{ij}. During computation, we ensure that the eigenvalues of the HFB-Popov matrix are real as there are no topological defects present in the system.

B. Mode evolution of the trapped TBEC at $T = 0$ K

Under the HFB-Popov approximation, the excitation spectrum of the TBEC in an optical lattice is gapless for the SF phase, while it has a finite gap for the MI phase [10]. In the SF phase, spontaneous symmetry breaking at condensation results in two Goldstone modes, one each for the two species. The number of Goldstone modes, however, depends on whether the system is in the miscible or immiscible phase, and the geometry of the density distributions. To explore different possibilities, as mentioned earlier, we consider two different TBEC systems. These are binary mixtures which can be driven from the miscible to the immiscible phase through the variation of the intra- or interspecies interaction using the Feshbach resonance. In particular, we consider ^{87}Rb-^{85}Rb [28,53] and ^{133}Cs-^{87}Rb [54,55] binary condensates as examples of the two cases, and study the mode evolution as the system approaches the immiscible from the miscible regime.

1. *Third Goldstone mode in the* ^{87}Rb-^{85}Rb *TBEC*

To examine the mode evolution with the tuning of the intraspecies interaction, we consider a quasi-1D TBEC consisting of ^{87}Rb and ^{85}Rb [28,53]. In this system, we consider ^{87}Rb and ^{85}Rb as the first and second species, respectively. The axial trapping frequency for both the species is $\omega_z = 2\pi \times 80$ Hz with 12.33 as the anisotropy parameter along the x and y directions. The laser wavelength used to create the optical lattice potential is $\lambda_L = 775$ nm. The numbers of atoms are $N_1 = N_2 = 100$, confined in 100 lattice sites superimposed on a harmonic potential. We choose the depth of the lattice potential $V_0 = 5E_R$ and set the tunneling matrix elements for the two species as $J_1 = 0.66E_R$ and $J_2 = 0.71E_R$, the intraspecies interaction U_{11} as $0.05E_R$, and the interspecies interaction U_{12} as $0.1E_R$. This set of DNLSE parameters is calculated by considering the width of the Gaussian beam as $0.3a$. Since the scattering length of ^{85}Rb is tunable with the Feshbach resonance [28], we study the excitation spectrum with variation in U_{22}. The evolution of the Kohn mode functions with the variation of U_{22} is shown in Fig. 1. For

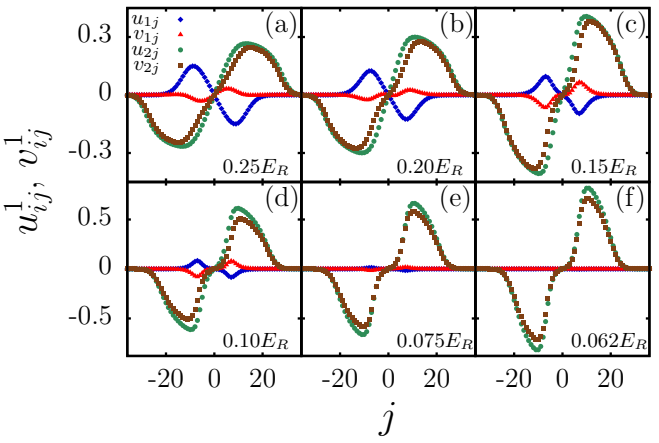

FIG. 1. (Color online) The evolution of the quasiparticle amplitudes corresponding to the ^{85}Rb Kohn mode as the intraspecies interaction of ^{85}Rb (U_{22}) is decreased from $0.25E_R$ to $0.062E_R$. (a),(b) When $U_{22} \geqslant 0.18E_R$, the system is in the miscible phase and the Kohn mode ($l = 1$) has contributions from both the species. (c)–(e) When the system is on the verge of phase separation, then the Kohn mode of ^{85}Rb goes soft. (f) At phase separation $U_{22} \leqslant 0.065E_R$ the Kohn mode transforms into a Goldstone mode.

$0.18 \leqslant U_{22} \leqslant 0.25E_R$, the system is in the miscible domain, and the Kohn mode is a linear combination of the ^{87}Rb and ^{85}Rb Kohn modes. As we approach phase separation by reducing the value of U_{22}, we observe a decrease in the Kohn mode amplitude of ^{87}Rb component and the mode function of ^{85}Rb becomes soft at $0.062E_R$. The softening of the mode is evident from the evolution of the mode energies as shown in Fig. 2(a). The figure shows that the mode continues as the third Goldstone mode for $U_{22} \leqslant 0.062E_R$. The emergence of the third Goldstone mode is associated with a change in the geometry of the system; the density changes from the overlapping to a sandwich profile as shown in Figs. 3(a)–3(c). Thus, as discussed in our earlier work [46], the binary condensate is separated into three distinct subcomponents.

2. *Third Goldstone mode in the* ^{133}Cs-^{87}Rb *TBEC*

For mode evolution with tuning of the interspecies interaction, we consider the binary system of Cs-Rb [54,55]. Here, we consider ^{133}Cs and ^{87}Rb as the first and second species, respectively. To study the mode evolution as the system undergoes the transition from the miscible to the immiscible phase, the interspecies interaction U_{12} is varied, which is possible using the magnetic Feshbach resonance [56]. The parameters of the system considered are $N_1 = N_2 = 100$ with similar trapping frequencies as in the case of the ^{87}Rb-^{85}Rb mixture. The lattice parameters are chosen as $J_1 = 0.92E_R$, $J_2 = 1.95E_R$, $U_{11} = 0.40E_R$, and $U_{22} = 0.21E_R$. At $U_{12} = 0$, the two condensates are uncoupled and have two Goldstone modes, one corresponding to each of the two species. At low values of U_{12}, in the miscible regime, the condensate density profiles of the two species overlap as shown in Fig. 3(d). As we increase U_{12}, the Kohn mode of ^{87}Rb gradually goes soft and at a critical value $U^c_{12} = 0.3E_R$ it is transformed into the third Goldstone mode. For $U^c_{12} < U_{12}$, the geometry of the condensate density profile changes and acquires a sandwich

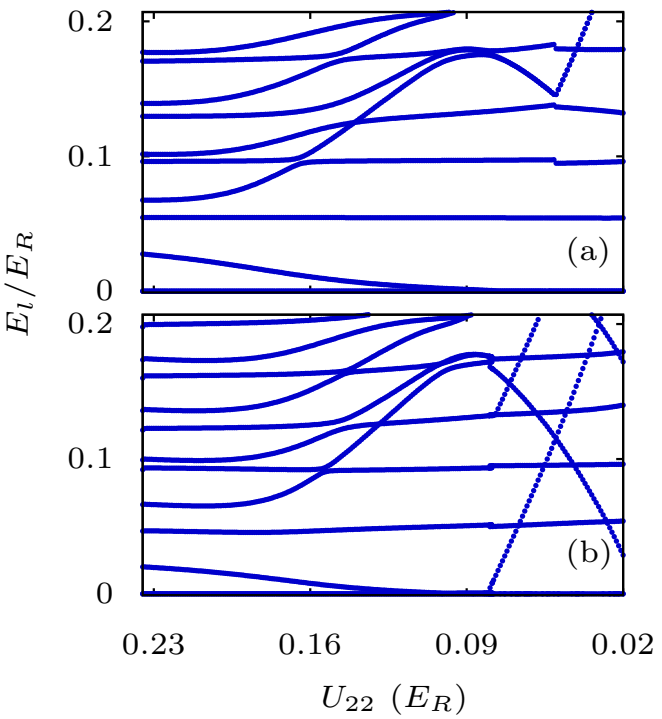

FIG. 2. (Color online) The evolution of the low-lying modes as a function of the intraspecies interaction of the ^{85}Rb (U_{22}) in the ^{87}Rb-^{85}Rb TBEC held in quasi-1D optical lattices. Excitation spectrum (a) at zero temperature and (b) in the presence of quantum fluctuations. Here U_{22} is in units of the recoil energy E_R.

structure in which the Cs condensate (higher mass) is at the center and flanked by the Rb condensate (lower mass) at the edges as shown in Fig. 3(f). This is also evident from the evolution of the low-lying modes, shown in Fig. 4(a), and is reflected in the structural evolution of the quasiparticle amplitudes in Fig. 5. Hence the system attains an extra Goldstone mode after transition from a miscible- to a sandwich-type profile.

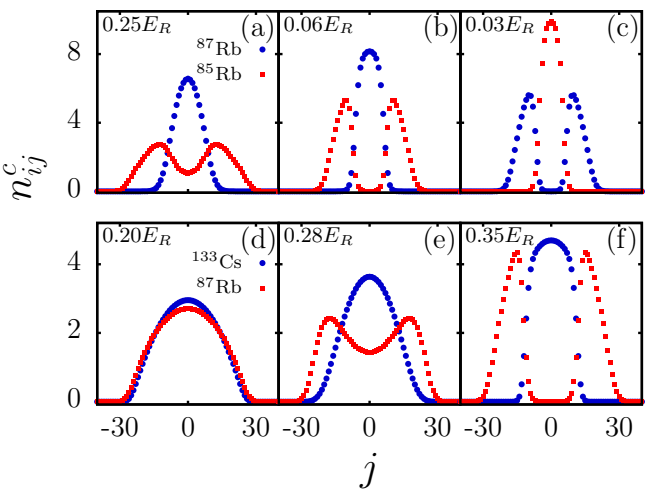

FIG. 3. (Color online) The geometry of the condensate density profiles and its transition from the miscible to the immiscible regime. (a)–(c) The transition from the miscible to the *sandwich* profile for the ^{87}Rb-^{85}Rb TBEC with change in the intraspecies interaction U_{22} at $T = 0$ K. The position exchange (c) in the sandwich profile occurs at $U_{11} = U_{22} = 0.05E_R$. (d)–(f) show similar condensate density profiles for the Cs-Rb TBEC with change in the interspecies interaction U_{12} at $T = 0$ K. In this system the transition to the sandwich geometry occurs at $U_{12}^c = 0.3E_R$.

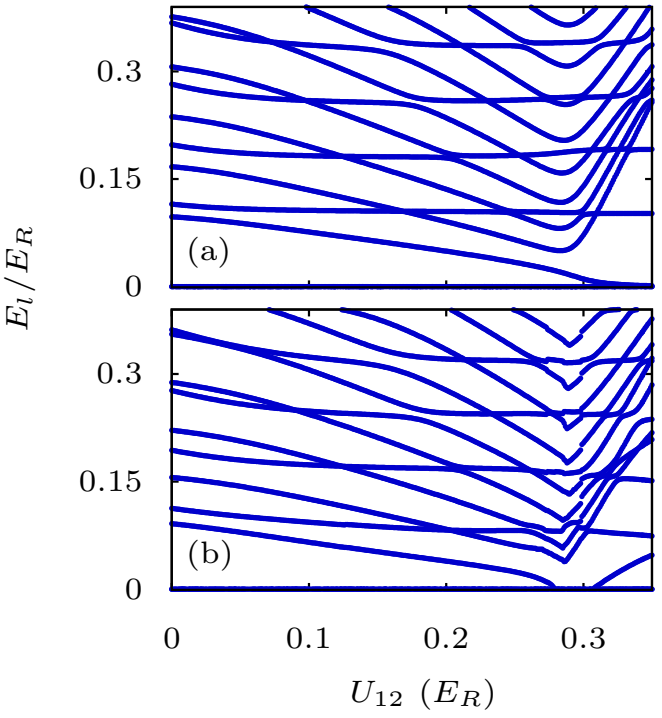

FIG. 4. (Color online) The evolution of the energies of the low-lying modes as a function of the interspecies interaction (U_{12}) in Cs-Rb TBEC held in a quasi-1D lattice potential. The excitation spectrum (a) at $T = 0$ K, and (b) after including the quantum fluctuations. Here U_{12} is in units of the recoil energy E_R.

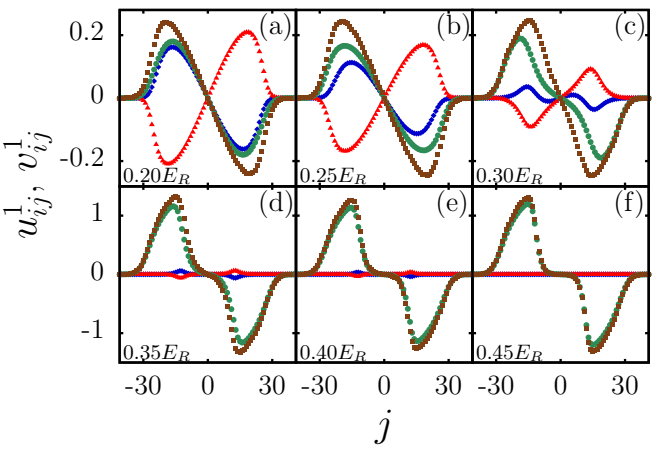

FIG. 5. (Color online) The evolution of the quasiparticle amplitudes corresponding to the Kohn mode as the interspecies interaction is increased from $0.2E_R$ to $0.35E_R$ for a Cs-Rb TBEC in a quasi-1D lattice potential at $T = 0$ K. (a)–(c) In the miscible regime, the Kohn mode has contributions from both species. (d)–(f) For $U_{12} > 0.3E_R$ the Kohn mode of ^{87}Rb goes soft, whereas that of ^{133}Cs decreases in amplitude.

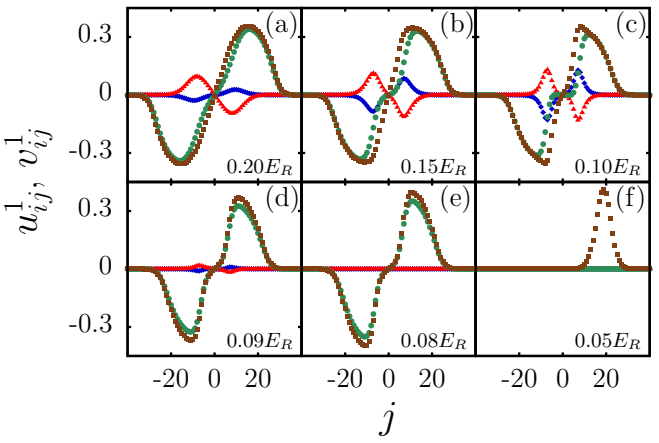

FIG. 6. (Color online) The evolution of the quasiparticle amplitudes corresponding to the Kohn mode for ^{87}Rb-^{85}Rb TBEC in the presence of the fluctuations as the intraspecies interaction of ^{85}Rb (U_{22}) is decreased from $0.2E_R$ to $0.05E_R$. (a)–(e) The Kohn mode of ^{85}Rb goes soft, whereas that of ^{87}Rb decreases in amplitude and finally vanishes in (e). (f) The sloshing mode, which emerges after phase separation as the sandwich density profile transforms into a *side-by-side* profile.

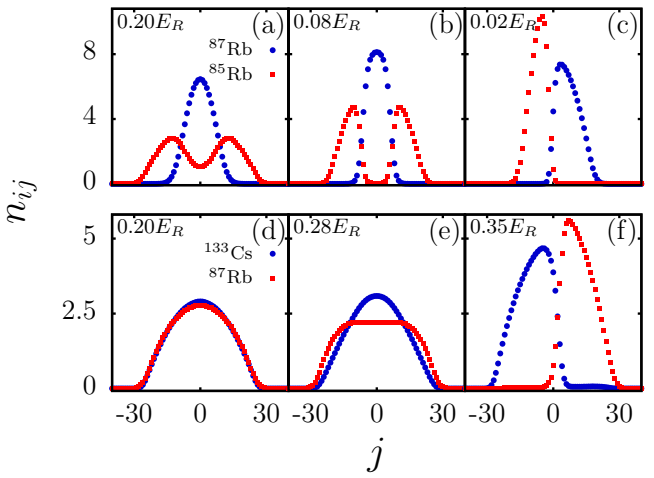

FIG. 7. (Color online) The fluctuation-induced transition in the geometry of the total density profile (condensate + quantum fluctuations) of a TBEC at $T = 0$ K in a quasi-1D lattice potential. (a)–(c) The transition in the ^{87}Rb-^{85}Rb system from the miscible to the sandwich and finally to the side-by-side profile with change in the intraspecies interaction. (d), (e) The transition in the Cs-Rb TBEC from the miscible to the side-by-side profile with change in the interspecies interaction U_{12}. The geometry of the ground state of both systems in the immiscible regime is different from that at zero temperature in the absence of the fluctuations, Fig. 3.

3. *Position exchange of species*

A remarkable feature in the evolution of the condensate density profiles of an ^{87}Rb-^{85}Rb TBEC with variation of U_{22} is the observation of position exchange in the immiscible domain. This is absent when the trapping potential consists of only a harmonic potential (continuous system), and is the result of the discrete symmetry associated with the optical lattice. As discussed earlier, in this system we fix U_{11} and U_{12} and vary U_{22} (the intraspecies interaction of ^{85}Rb). At higher values of U_{22} the TBEC is in the miscible phase, and as we decrease U_{22}, at the critical value $U^c_{22} = 0.17E_R$ the TBEC enters the immiscible domain. The geometry of the density profiles is of sandwich type and the component with smaller U_{ii} is at the center. An example of a condensate density profile in this domain, $U_{22} = 0.06E_R$, is shown in Fig. 3(b). In the figure, the species with smaller intraspecies interaction (^{87}Rb) is at the center and ^{85}Rb is at the edges. As U_{22} is further decreased, the system continues to be in the same phase. During evolution, an instability arises when both intraspecies interactions are the same ($U_{11} = U_{22} = 0.05$). At this value of U_{22} the components exchange their places in the trap. This is also reflected in the excitation spectrum; a discontinuity at $U_{22} = 0.05E_R$ in the plot of the mode evolution shown in Fig. 2(a) is a signature of the instability. On further decrease of U_{22}, we enter the $U_{22} < U_{11}$ domain and ^{85}Rb occupies the center of the trap. An example of the density profiles in this domain, $U_{22} = 0.03$, is shown in Fig. 3(c). The position exchange, however, does not occur in the Cs-Rb system as in that case we vary U_{12}.

C. Effect of quantum fluctuations

We compute the condensate profiles and modes for the ^{87}Rb-^{85}Rb TBEC, including the effect of quantum fluctuations. We then encounter severe oscillations in the number of atoms during the iterations used to solve the DNLSEs and there is no convergence. To mitigate this, we use a successive under-relaxation technique with $r^{\rm un} = 0.6$. For computations, we consider the same set of parameters as in the case of $T = 0$ K without fluctuations. The fluctuations break the spatial symmetry of the system as we vary the intraspecies interaction of ^{85}Rb (U_{22}). In the immiscible domain, the condensate density profile changes from the sandwich to the side-by-side profile at $0.078E_R$. The system acquires a new stable ground state as the chemical potential of the system decreases from $0.92E_R$ to $0.80E_R$. The evolution of the mode energies with U_{22} including the fluctuation is shown in Fig. 2(b). It is evident that at this value $U_{22} = 0.078E_R$, the ^{85}Rb Kohn mode goes soft and emerges as a sloshing mode. The transformations in the mode functions as U_{22} is decreased about this point are shown in Fig. 6. This topological phase transition is evident from the density profiles of the TBEC in the presence of quantum fluctuations as shown in Figs. 7(a)–7(c).

In the Cs-Rb system, due to quantum fluctuations, the Kohn mode of ^{87}Rb goes soft at a lower value of U_{12} compared to the value without fluctuations. This is evident in the mode evolution with quantum fluctuations as shown in Fig. 4(b). The discontinuity in the spectrum is the signature of the transition from the miscible to the immiscible regime. The soft Kohn mode gains energy and gets hard at $0.31E_R$. This mode hardening is due to the topological change in the ground-state density profile from the miscible to the side-by-side profile, shown in Figs. 7(d)–7(f). The lowest mode with nonzero excitation energy corresponding to the side-by-side profile is shown in Figs. 8(e) and 8(f).

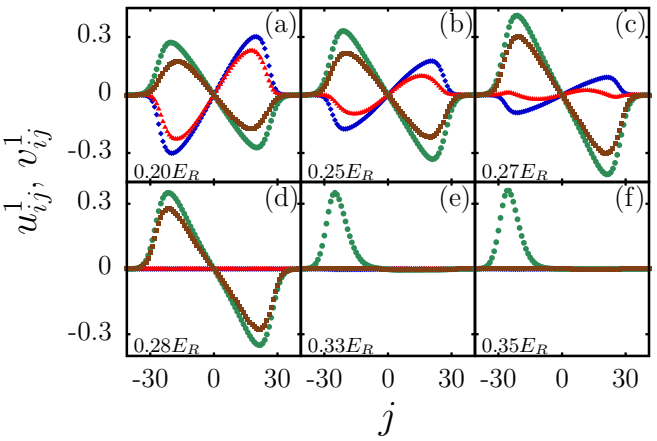

FIG. 8. (Color online) The evolution of the quasiparticle amplitude corresponding to the Kohn mode for the Cs-Rb TBEC in the presence of fluctuations. (a)–(d) The Kohn mode evolves as the interspecies interaction is increased. (e),(f) It is transformed into a sloshing mode as the TBEC acquires the side-by-side density profile after phase separation.

V. CONCLUSIONS

We have studied the ground-state density profiles and the excitation spectrum of TBECs in quasi-1D optical lattices. We observe that the system gains an additional Goldstone mode at phase separation at zero temperature. Furthermore, in a TBEC where a miscible to immiscible transition is driven through variation of the intraspecies interaction (^{87}Rb-^{85}Rb), a finite discontinuity in the excitation energy spectra is observed in the neighbourhood of equal intraspecies interaction strengths. In the presence of quantum fluctuations, on varying the intraspecies interaction of ^{85}Rb, in the immiscible regime, the ground-state density profiles transform from sandwich to side-by-side geometry. This is characterized by the hardening of the Kohn mode which emerges as a sloshing mode. The fluctuation-induced topological change from a completely miscible to a side-by-side ground-state density profile is also evident in a ^{133}Cs-^{87}Rb mixture. Our current studies show that the geometry of the density profiles with and without quantum fluctuations is different. Since quantum fluctuations are present in experiments, it is crucial to include quantum fluctuations to obtain the correct density profiles of TBECs in optical lattices in the phase-separated domain.

ACKNOWLEDGMENTS

We thank S. Gautam and S. Chattopadhyay for useful discussions. The results presented in the paper are based on computations using the 3TFLOP HPC cluster at the Physical Research Laboratory, Ahmedabad, India. We also thank the anonymous referee for the thorough review and valuable comments, which contributed to improving the quality of the paper.

[1] M. A. Cazalilla, R. Citro, T. Giamarchi, E. Orignac, and M. Rigol, Rev. Mod. Phys. **83**, 1405 (2011).
[2] E. H. Lieb and W. Liniger, Phys. Rev. **130**, 1605 (1963).
[3] O. Morsch and M. Oberthaler, Rev. Mod. Phys. **78**, 179 (2006).
[4] I. Bloch, J. Dalibard, and W. Zwerger, Rev. Mod. Phys. **80**, 885 (2008).
[5] S. Friebel, C. D'Andrea, J. Walz, M. Weitz, and T. W. Hänsch, Phys. Rev. A **57**, R20 (1998).
[6] L. Guidoni and P. Verkerk, Phys. Rev. A **57**, R1501 (1998).
[7] B. Paredes, A. Widera, V. Murg, O. Mandel, S. Folling, I. Cirac, G. V. Shlyapnikov, T. W. Hansch, and I. Bloch, Nature (London) **429**, 277 (2004).
[8] I. Bloch, Nat. Phys. **1**, 23 (2005).
[9] S. Sachdev, *Quantum Phase Transitions* (Cambridge University Press, New York, 2011).
[10] M. Greiner, O. Mandel, T. Esslinger, T. W. Hansch, and I. Bloch, Nature (London) **415**, 39 (2002).
[11] H. Moritz, T. Stöferle, M. Köhl, and T. Esslinger, Phys. Rev. Lett. **91**, 250402 (2003).
[12] T. Stöferle, H. Moritz, C. Schori, M. Köhl, and T. Esslinger, Phys. Rev. Lett. **92**, 130403 (2004).
[13] B. Laburthe Tolra, K. M. O'Hara, J. H. Huckans, W. D. Phillips, S. L. Rolston, and J. V. Porto, Phys. Rev. Lett. **92**, 190401 (2004).
[14] C. Orzel, A. K. Tuchman, M. L. Fenselau, M. Yasuda, and M. A. Kasevich, Science **291**, 2386 (2001).
[15] M. Greiner, I. Bloch, O. Mandel, T. W. Hänsch, and T. Esslinger, Phys. Rev. Lett. **87**, 160405 (2001).
[16] C. Fort, F. S. Cataliotti, L. Fallani, F. Ferlaino, P. Maddaloni, and M. Inguscio, Phys. Rev. Lett. **90**, 140405 (2003).
[17] C. D. Fertig, K. M. O'Hara, J. H. Huckans, S. L. Rolston, W. D. Phillips, and J. V. Porto, Phys. Rev. Lett. **94**, 120403 (2005).
[18] L. Fallani, L. De Sarlo, J. E. Lye, M. Modugno, R. Saers, C. Fort, and M. Inguscio, Phys. Rev. Lett. **93**, 140406 (2004).
[19] S. Burger, F. S. Cataliotti, C. Fort, F. Minardi, M. Inguscio, M. L. Chiofalo, and M. P. Tosi, Phys. Rev. Lett. **86**, 4447 (2001).
[20] F. S. Cataliotti, S. Burger, C. Fort, P. Maddaloni, F. Minardi, A. Trombettoni, A. Smerzi, and M. Inguscio, Science **293**, 843 (2001).
[21] M. Krämer, C. Menotti, L. Pitaevskii, and S. Stringari, Eur. Phys. J. D **27**, 247 (2003).
[22] E. Lundh, Phys. Rev. A **70**, 033610 (2004).
[23] J.-P. Martikainen and H. T. C. Stoof, Phys. Rev. A **68**, 013610 (2003).
[24] A. M. Rey, G. Pupillo, C. W. Clark, and C. J. Williams, Phys. Rev. A **72**, 033616 (2005).
[25] A. M. Rey, Ultracold bosonic atoms in optical lattices, Ph.D. thesis, University of Maryland, 2004.
[26] M. P. A. Fisher, P. B. Weichman, G. Grinstein, and D. S. Fisher, Phys. Rev. B **40**, 546 (1989).
[27] R. Navarro, R. Carretero-González, and P. G. Kevrekidis, Phys. Rev. A **80**, 023613 (2009).
[28] S. B. Papp, J. M. Pino, and C. E. Wieman, Phys. Rev. Lett. **101**, 040402 (2008).
[29] S. Tojo, Y. Taguchi, Y. Masuyama, T. Hayashi, H. Saito, and T. Hirano, Phys. Rev. A **82**, 033609 (2010).

[30] S. Gautam and D. Angom, J. Phys. B **44**, 025302 (2011).
[31] S. Gautam and D. Angom, Phys. Rev. A **81**, 053616 (2010).
[32] T. Kadokura, T. Aioi, K. Sasaki, T. Kishimoto, and H. Saito, Phys. Rev. A **85**, 013602 (2012).
[33] C. Ticknor, Phys. Rev. A **88**, 013623 (2013).
[34] D. Gordon and C. M. Savage, Phys. Rev. A **58**, 1440 (1998).
[35] J. Catani, L. De Sarlo, G. Barontini, F. Minardi, and M. Inguscio, Phys. Rev. A **77**, 011603 (2008).
[36] B. Gadway, D. Pertot, R. Reimann, and D. Schneble, Phys. Rev. Lett. **105**, 045303 (2010).
[37] G.-H. Chen and Y.-S. Wu, Phys. Rev. A **67**, 013606 (2003).
[38] A. B. Kuklov and B. V. Svistunov, Phys. Rev. Lett. **90**, 100401 (2003).
[39] A. Kuklov, N. Prokof'ev, and B. Svistunov, Phys. Rev. Lett. **92**, 050402 (2004).
[40] M.-C. Cha, Int. J. Mod. Phys. B **27**, 1362002 (2013).
[41] F. Zhan and I. P. McCulloch, Phys. Rev. A **89**, 057601 (2014).
[42] T. Mishra, R. V. Pai, and B. P. Das, Phys. Rev. A **76**, 013604 (2007).
[43] Y.-C. Kuo and S.-F. Shieh, J. Math. Anal. Appl. **347**, 521 (2008).
[44] J. Ruostekoski and Z. Dutton, Phys. Rev. A **76**, 063607 (2007).
[45] A. Griffin, Phys. Rev. B **53**, 9341 (1996).
[46] A. Roy, S. Gautam, and D. Angom, Phys. Rev. A **89**, 013617 (2014).
[47] A. Roy and D. Angom, Phys. Rev. A **90**, 023612 (2014).
[48] M. L. Chiofalo, M. Polini, and M. P. Tosi, Eur. Phys. J. D **11**, 371 (2000).
[49] D. Jaksch, C. Bruder, J. I. Cirac, C. W. Gardiner, and P. Zoller, Phys. Rev. Lett. **81**, 3108 (1998).
[50] G. Baym and C. J. Pethick, Phys. Rev. Lett. **76**, 6 (1996).
[51] E. Anderson, Z. Bai, C. Bischof, S. Blackford, J. Demmel, J. Dongarra, J. D. Croz, A. Greenbaum, S. Hammarling, A. McKenney, and D. Sorensen, *LAPACK Users' Guide*, 3rd ed. (Society for Industrial and Applied Mathematics, Philadelphia,1999).
[52] T. P. Simula, S. M. M. Virtanen, and M. M. Salomaa, Comput. Phys. Commun. **142**, 396 (2001).
[53] S. Händel, T. P. Wiles, A. L. Marchant, S. A. Hopkins, C. S. Adams, and S. L. Cornish, Phys. Rev. A **83**, 053633 (2011).
[54] D. J. McCarron, H. W. Cho, D. L. Jenkin, M. P. Köppinger, and S. L. Cornish, Phys. Rev. A **84**, 011603 (2011).
[55] A. Lercher, T. Takekoshi, M. Debatin, B. Schuster, R. Rameshan, F. Ferlaino, R. Grimm, and H.-C. Ngerl, Eur. Phys. J. D **65**, 3 (2011).
[56] K. Pilch, A. D. Lange, A. Prantner, G. Kerner, F. Ferlaino, H.-C. Nägerl, and R. Grimm, Phys. Rev. A **79**, 042718 (2009).